Available online at www.sciencedirect.com

ScienceDirect

Procedia Structural Integrity 21 (2019) 224–232

Structural Integrity Procedia

www.elsevier.com/locate/procedia

1st International Workshop on Plasticity, Damage and Fracture of Engineering Materials

Morphology and Grain Orientation Dependent Localization and Necking in Dual-phase Steels

Serhat Onur Çakmak, Tuncay Yalçinkaya*

Department of Aerospace Engineering, Middle East Technical Universty, Ankara 06800, Turkey

Abstract

This paper studies the plastic deformation, localization and the necking behavior of polycrystalline dual phase (DP) steels, with different martensite volume fractions, and ferrite orientation distributions, through crystal plasticity finite element method. The grain structure of the full size micron-scale polycrystalline samples is built through Voronoi tesselation and the specimens are deformed under uniaxial loading condition. For the modelling of martensite phase J2 plasticity with isotropic hardening is employed while in randomly oriented ferrite grains the crystal plasticity theory works. The material parameters are identified with respect to uniaxial tensile experimental data using a fully periodic RVE with enough number of ferrite grains. The attention is focused on the effect of the martensite morphology and the ferrite orientation distribution on the formation of the shear bands and then the necking of the sample.

Keywords: Dual-Phase Steel; Crystal Plasticity; Necking; Shear Bands

1. Introduction

Initially developed in 1970s, DP steels have been used frequently in automotive industry, thanks to its low yield stress, moderate strain hardening capacity, high tensile strength and continuous yield behavior. In order to improve the application range and the mechanical properties of DP steels, substantial research have focused on their micro level investigations due to their interesting microstructure which does not only offer mechanical improvement but also some specific degradation mechanisms (see e.g. Kadkhodapour et al. (2011b); Vajragupta et al. (2014); Zecevic et al. (2016); Diehl et al. (2017)). Therefore, the macroscopic behavior is strictly relevant to microstructural parameters such as martensite volume fraction, carbon content of martensite, ferrite grain size (see e.g. Jiang et al. (1995); Bag

* Corresponding author. Tel.: +90-312-210-4258 ; fax: +90-312-210-4250.
E-mail address: yalcinka@metu.edu.tr

2452-3216
10.1016/j.prostr.2019.12.105

et al. (1999); Pierman et al. (2014); Tasan et al. (2014)). In addition to these parameters, martensite morphology affects strongly the mechanical properties such as strain hardening and necking deformability (Park et al., 2014).

From the macroscopic point of view, dual phase steels show homogeneous and uniform deformation like many metallic materials. However, from the micromechanical perspective, plastic deformation of DP steels shows naturally heterogeneous behavior because of microstructural inhomogeneity at the grain level. The main source of this inhomogeneity is the incompatibility of deformation between the hard martensite phase and the soft plastically deforming ferrite phase. Compared to martensite phase, deformation of the ferrite phase occurs at a high rate and due to inhomogeneous strain distribution between ferrite and martensite(Shen et al., 1986). Although there are various studies focussing on the effect of martensite distribution and morphology on the strain localization and damage initiation (see e.g. Kadkhodapour et al. (2011a)) in dual phase steels, there is still need for further detailed analyses considering the effect of different microstructural features together (see e.g. Choi et al. (2013); Woo et al. (2012)). In addition to mechanical differences between martensite and ferrite phases, initial crystallographic orientation of ferrite phase and the distribution of martensite phase in DP microstructure affects significantly the microscopic deformation, stress-strain partitioning, and the failure.

In this study the effect of microstructural features of ferrite and martensite phases are investigated through the crystal plasticity finite element method (CPFEM). In order to realize this, eight artificial polycrystalline dual phase micro-specimens with four different martensite volume fraction and two different martensite morphology are studied. The numerical analysis of these specimen is conducted under uniaxial tensile loading condition using crystal plasticity and J2 plasticity with isotropic hardening models for ferrite and martensite phases, respectively. As a result of these simulations, the effect of different martensite distributions and initial ferrite orientations on the formation of shear bands, and necking behavior is discussed detail, which has not been done in the literature before.

2. Artificial Micro-Specimen Generation

For the numerical analysis, four different artificial uniaxial tensile specimens are generated by polycrystal generation and meshing software Neper (see Quey et al. (2011)). They have rectangular cross-section of 25 μm $\times$ 25 μm and length of 100 μm. Each of these specimens include in total 500 grains with different martensite volume fractions. The volume fractions of martensite phase is chosen as 15%, 19%, 28% and 37% to be consistent with the DP steels presented in Lai et al. (2016), which is used for material parameter identification. The DP steels with regarding volume fractions are referred to as VF15, VF19, V28, and VF37 respectively in this work. The microstructural characteristics of the materials is presented in Table 1, where d_f, d_m, V_m represent the average grain size of ferrite phase, the average grain size of martensite phase the martensite volume fraction respectively.

Table 1: Microstructural characteristics of investigated dual-phase steels (from Lai et al. (2016))

Steel	V_m (%)	d_f (μm)	d_m (μm)
VF15	15	6.5	1.2
VF19	19	5.9	1.5
VF28	28	5.5	2.1
VF37	37	4.2	2.4

Moreover, two different morphologies, which are referred to as Moph1 and Morp2 are generated for each micro-specimen with different volume fraction in order to study the influence of morphology as presented in Figure 1. White areas in each micro-specimen show martensite grains, while green areas in each micro-specimen show ferrite grains. Quasi-static uniaxial tensile loading (with $\dot{\varepsilon} = 10^{-3}\ s^{-1}$) is applied for each specimen which is discretized with 10 noded tetrahedral C3D10 elements in ABAQUS.

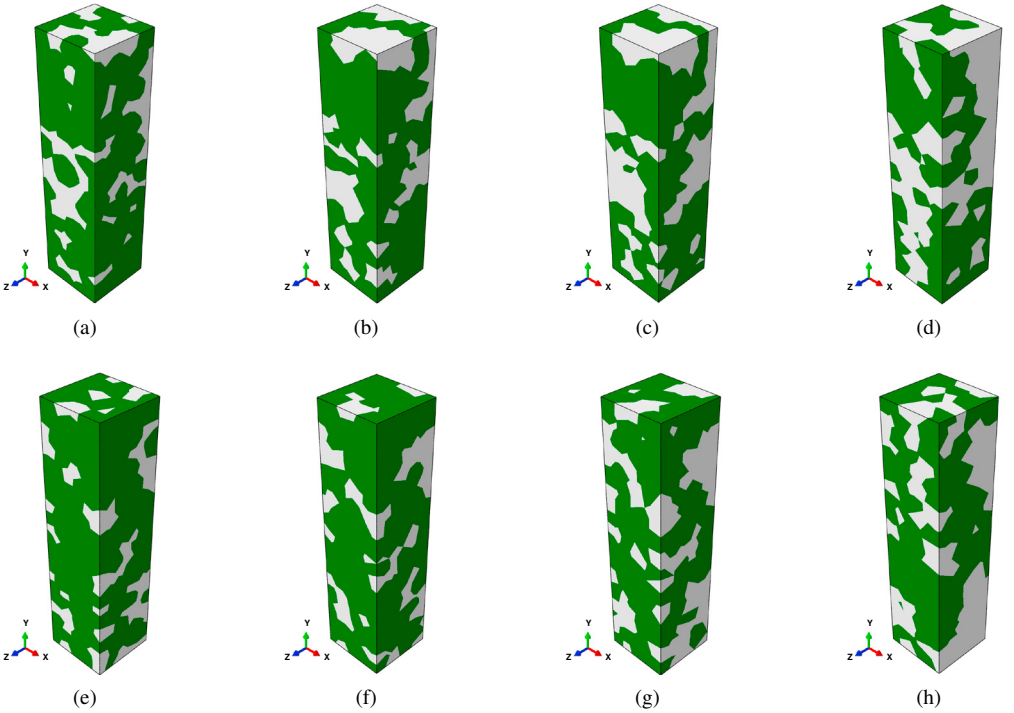

Fig. 1: Dual-phase specimen with different morphologly and volume fraction of martensite. **(a)** VF15-Morph1, **(b)** VF19-Morph1, **(c)** VF28-Morph1, **(d)** VF37-Morph1, **(e)** VF15-Morph2, **(f)** VF19-Morph2, **(g)** VF28-Morph2 and **(h)** VF37-Morph2

3. Constitutive Models

In this section the constitutive frameworks for the modeling of plasticity behavior of both martensite and ferrite phases is presented very shortly.

3.1. J2 Plasticity Modeling of Martensite Phase

In the numerical analyses rate-independent von Mises plasticity theory with isotropic hardening is assigned to martensite grains, whose flow behavior is modeled by the phenomenological equations and parameter sets given by Pierman et al. (2014),

$$\sigma_{y,m} = \sigma_{y0,m} + k_m(1 - exp(-\varepsilon_P n_m)) \tag{1}$$

where $\sigma_{y,m}$ is the current yield stress, ε_P is the accumulated plastic strain, and $\sigma_{y0,m}$, k_m, n_m are material parameters. C_m is the martensite carbon content in wt%, whose influence on the strain hardening is given below

$$\sigma_{y0,m} = 300 + 1000 C_m^{1/3}. \tag{2}$$

The hardening modulus k_m reads

$$k_m = \frac{1}{n_m}\left[a + \frac{bC_m}{1 + \left(\frac{C_m}{C_0}\right)^q}\right] \tag{3}$$

with a=33 GPa, b=36 GPa, C_0=0.7, q=1.45, n_m=120, C_m=0.3 wt%. In the calculations Young's modulus and Poissons ratio are taken as E=210GPa and ν=0.3.

3.2. Crystal Plasticity Modeling of Ferrite Phase

While martensite phase deforms according to J2 flow theory the ferrite phase is modeled with the local, rate dependent crystal plasticity framework (see Huang (1991)), which considers the anisotropy due to ferrite grain orientation distribution. The framework is based on the multiplicative decomposition of deformation gradient into an elastic and a plastic part, $\boldsymbol{F} = \boldsymbol{F}^e \boldsymbol{F}^p$. The plastic deformation gradient is obtained through the integration of the plastic velocity gradient which is attained via the summation of plastic slip rate on each slip system which evolves according to the following power law,

$$\dot{\gamma}^{(\alpha)} = \dot{\gamma}_0 \left| \frac{\tau^{(\alpha)}}{g^{(\alpha)}} \right|^{1/m} \text{sign}(\tau^{(\alpha)}) \tag{4}$$

where, $\dot{\gamma}_0$ is a reference slip rate, $\tau^{(\alpha)}$ is the Schmid resolved shear stress which is the projection of the Kirchhoff stress on the slip systems, $g^{(\alpha)}$ is the slip resistance on slip system α which governs the hardening of the single crystal, and m is the rate sensitivity parameter. Hardening is governed by

$$\dot{g}^{(\alpha)} = \sum_{\beta=1} h^{\alpha\beta} \left| \dot{\gamma}^{\beta} \right| \tag{5}$$

where $h^{\alpha\beta}$ is the latent hardening matrix. This matrix measures the strain hardening due to shearing of slip system β on slip system α and it is defined as

$$h^{\alpha\beta} = q^{\alpha\beta} h^{\alpha\alpha} \tag{6}$$

where $q^{\alpha\beta}$ is the latent hardening matrix and $h^{(\beta)}$ represents the self-hardening rate, for which a simple form is used (see e.g. (Peirce et al., 1982)),

$$h^{\alpha\alpha} = h_0 \text{sech}^2 \left| \frac{h_0 \gamma}{g_s - g_0} \right| \tag{7}$$

where g_0 is the initial slip resistance, h_0 is the initial hardening modulus, and g_s is the saturation value of the slip resistance. These relations summarizes the main equations for the calculation of plastic slip in each slip system in single crystal plasticity framework. Due to the orientation difference in each grain the Schmid resolved shear stress would be different as well which would result in different plastic slip and stress evolution in each crystal and stress concentration at the grain boundaries. For more details on the plastic strain decomposition, the incremental calculation of plastic strain and stress the readers are referred to the literature (see e.g. Huang (1991); Yalcinkaya et al. (2008). The single crystal plasticity model runs in each grain that is generated by Voronoi tesselation with Neper software.

The crystal plasticity hardening parameters of ferrite phase is obtained through an artificial representative volume element (RVE), which is created through Neper and deformed under uniaxial tensile loading. Simulations are conducted with the RVE under periodic boundary conditions and crystal plasticity hardening parameters are fitted to the experimental data in Lai et al. (2016) as shown in Figure 2. Only 12 slip systems are considered in these calculations (see e.g. Yalcinkaya et al. (2009) and Yalcinkaya et al. (2008) for details on BCC crystal plasticity). The resulting hardening parameters are presented in Table 2. For the cubic crystal symmetry parameters Fe data is used, C_{11} = 231.4GPa, C_{12} = 134.7GPa, and C_{12} = 116.4GPa (see e.g. Hosford (1993); Woo et al. (2012)).

Table 2: Calibrated crystal plasticity parameters for ferrite phase.

Steel	d_f μm	Slip System	g_s (MPa)	g_0 (MPa)	h_0 (MPa)
VF15	6.5	{112}⟨111⟩	252	98	475
VF19	5.9	{112}⟨111⟩	275	109	555
VF28	5.5	{112}⟨111⟩	306.6	118.5	802.8
VF37	4.2	{112}⟨111⟩	305	121.5	880

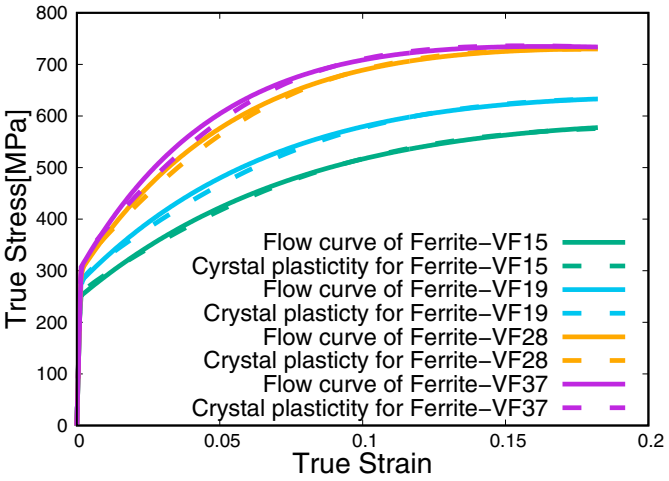

Fig. 2: CPFEM parameter identification through RVE calculations.

4. Results and Discussion

In this section the effect of martensite morphology and initial ferrite orientation distribution on the localization and necking behavior of micro specimen is studied through numerical examples using the parameters fitted with respect to experimental data.

Initial example addresses the influence of the martensite distribution on the necking behavior of micro specimens under uniaxial strain of 0.2 and 0.15 applied to 15%, 19% and 28%, 37% respectively. Same initial orientation sets were used for ferrite grains in each specimen. The contour plots of von Mises stress distribution on the deformed specimen with a y-z cross-sectional cut is presented in Figure 3 which includes two different martensite distribution for each specimen. It is clearly visible that the location of the necking depends highly on the martensite distribution. While in the initial case, which is presented in the first line, the necking location is close to the bottom of the specimen for all volume fractions in the second example the location approaches to the middle. Since the ferrite phase is more ductile than the martensite phase, the necking occurs in the regions with less martensite density. Moreover, martensite distribution affects also the macroscopic stress-strain response as illustrated in Figure 4. The influence of the martensite morphology on the macroscopic response is getting pronounced with increasing martensite content. In Figure 4 the response for VF15 and VF37 DP steels is presented which illustrates the fact that martensite morphology affects the ultimate tensile stress and strain value at which the necking starts, specially for the cases with high martensite volume fraction.

Next the effect of the initial ferrite grain orientation distribution is addressed for the initial martensite morphology which is referred to morph1 (Figure 1 (a)-(d)). For this study two different orientation sets, which are called oriset1 and oriset2 are assigned to the ferrite grains. The contour plots of von Mises stress distribution on the deformed specimen with a y-z cross-sectional cut is presented in Figure 5 which includes two different initial ferrite orientation distribution, that are plotted on to of each other for each DP case. It is shown that the location of the necking for specimens with 15%, 19% martensite volume fraction alters with the change of initial orientation distribution, while the results do not change for the samples with higher martensite volume fraction (28% and 37%). The macroscopic stress versus strain response for VF15 and VF 37 is presented in Figure 6. Due to the high number of ferrite grains, the macroscopic plastic response is not affected by the orientation distribution at the hardening regime of all specimens. However, there is a visible change in the softening response of low martensite content samples due to the change in the necking response presented in Figure 5. While the previous analysis on the effect of martensite distribution could be conducted with isotropic plasticity models, the current results showing the effect of microstructural parameters on localization and necking could only be analyzed though anisotropic grain level models such as crystal plasticity.

Last, the formation of shear bands at the onset of necking is discussed shortly. The accumulated plastic shear strain contour plots for certain cross-sectional cuts at the y-z plane are presented in Figure 7 for two different orientation

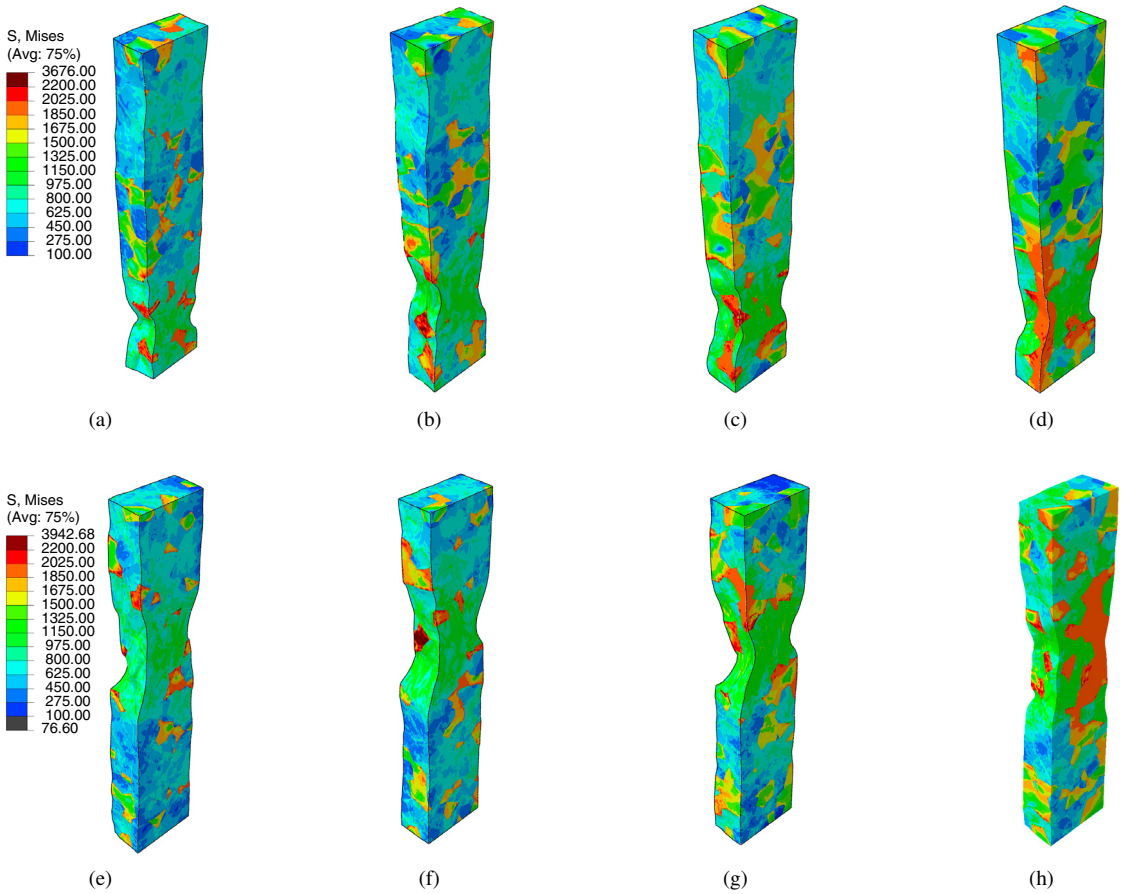

Fig. 3: Von Mises stress distribution for different morphology and volume fraction **(a-d)** morph1, **(e-h)** morph2 and **(a,e)** VF15,**(b,f)** VF19, **(c,g)** VF28, **(d,h)** VF37

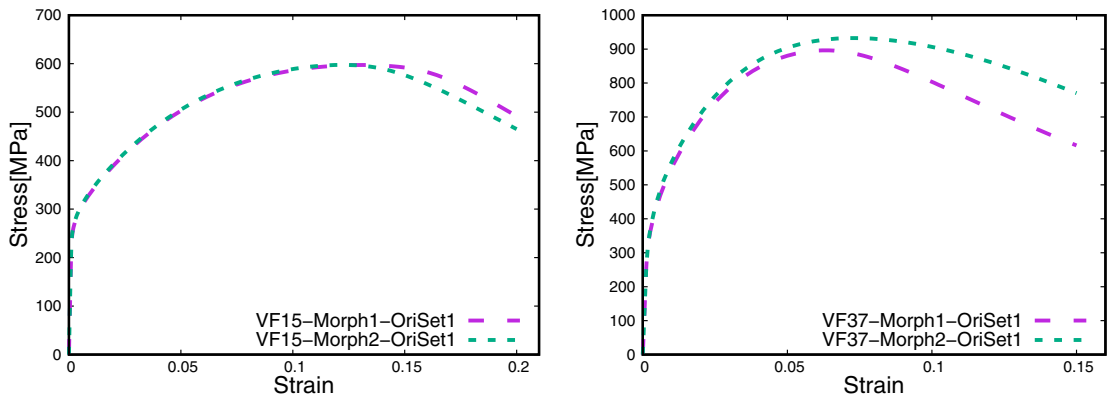

Fig. 4: Engineering stress-strain response of VF15 (left) and VF37 (right) for different martensite distributions.

sets of all DP steel specimens. Figure 7(a)-(d) shows the shear band formation at the onset of necking through oriset-1 while Figure 7(e)-(h) shows the shear band formation at the onset of necking through oriset-2. These figures should be compared with the necking results presented in Figure 5. As the necking location depends on the orientation set

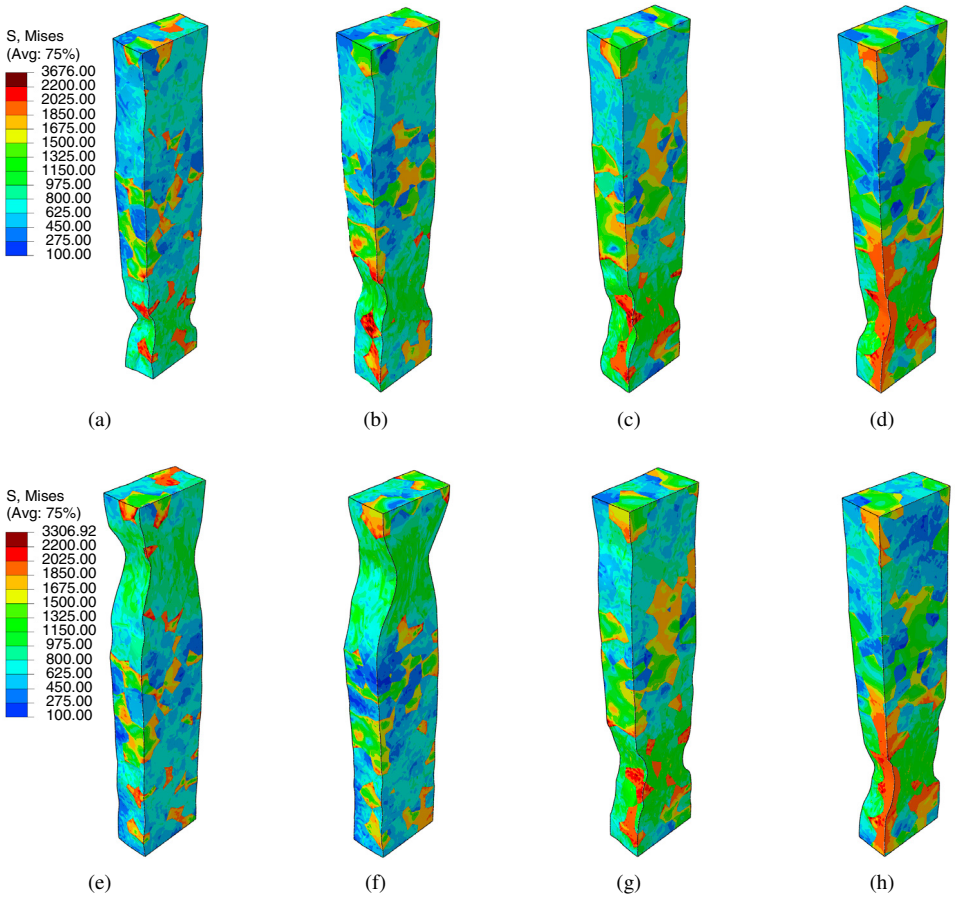

Fig. 5: Von Mises stress distribution for different orientation sets and volume fraction **(a-d)** orientation set1, **(e-h)** orientation set2 and **(a,e)** VF15,**(b,f)** VF19, **(c,g)** VF28, **(d,h)** VF37.

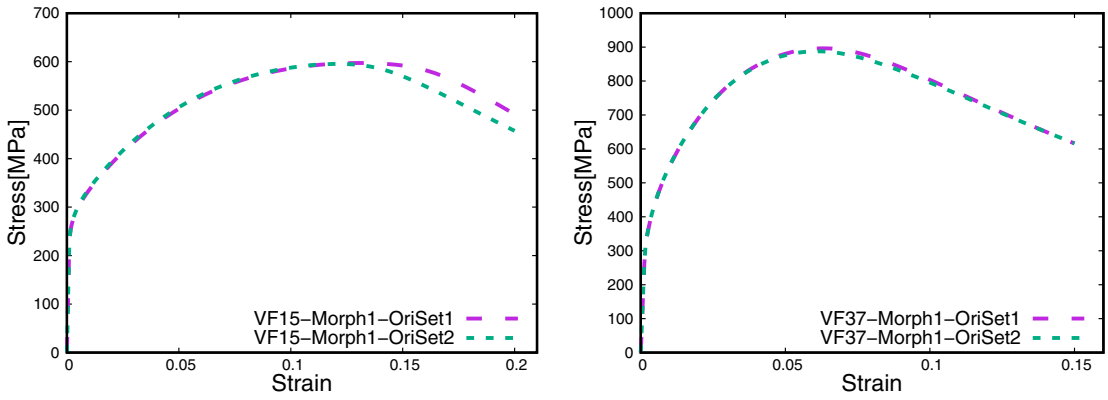

Fig. 6: Engineering stress-strain response of VF15 (left) and VF37 (right) for different initial ferrite orientation distributions.

for low martensite content cases, the difference in the formation of shear band like localization is also visible in these samples. Comparison of the localization in VF15 and VF19 presented in (a,e) and (b,f)) reveals this difference. For

the higher martensite content case the difference in the amount of accumulated plastic shear is visible rather than the location.

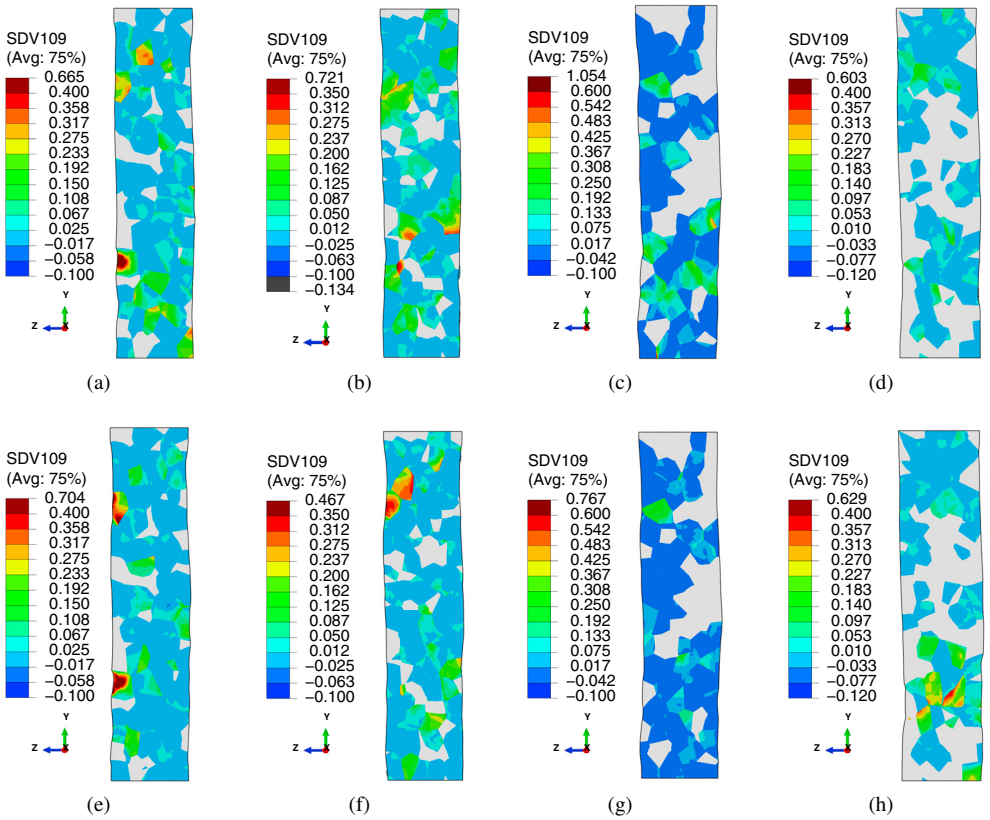

Fig. 7: The accumulated plastic shear strain at the onset of necking for different volume fraction and initial orientation sets **(a-d)** oriset1, **(e-h)** oriset2 and **(a,e)** VF15, **(b,h)** VF19, **(c,g)** VF28, **(d,h)** VF37.

5. Conclusions

The micron size specimens of different DP steels are investigated numerically through J2 plasticity and crystal plasticity theories for martensite and ferrite phases respectively. The attention is focussed on the localization and necking phenomena for specimen under uniaxial loading conditions. The effect of martensite grain distribution and initial ferrite grain orientation distribution is discussed in detail. The main conclusions are as follows,

- The location of the necking depends highly on the martensite distribution in micron sized specimen no matter what the volume fraction of the martensite is. The difference is also visible in the softening regime of macroscopic stress-strain responses, which becomes pronounced in the case with higher martensite volume fractions.
- The ferrite orientation distribution affects primarily the necking behavior of specimens with low martensite content in terms of both the necking location and the softening regime in stress-strain response.
- The shear band formation in the necking region depends also on the orientation distribution in the case with low martensite content which is consistent with the necking location.

References

Bag, A., Ray, K., Dwarakadasa, E., 1999. Influence of martensite content and morphology on tensile and impact properties of high-martensite dual-phase steels. Metallurgical and Materials Transactions A 30, 1193–1202. doi:https://doi.org/10.1007/s11661-999-0269-4.

Choi, S.H., Kim, E.Y., Woo, W., Han, S., Kwak, J., 2013. The effect of crystallographic orientation on the micromechanical deformation and failure behaviors of dp980 steel during uniaxial tension. International Journal of Plasticity 45, 85–102. doi:https://doi.org/10.1016/j.ijplas.2012.11.013.

Diehl, M., An, D., Shanthraj, P., Zaefferer, S., Roters, F., Raabe, D., 2017. Crystal plasticity study on stress and strain partitioning in a measured 3d dual phase steel microstructure. Physical Mesomechanics 20, 311–323. doi:10.1134/S1029959917030079.

Hosford, W., 1993. The mechanics of crystals and textured polycrystals. Oxford University Press.

Huang, Y., 1991. A user-material subroutine incroporating single crystal plasticity in the ABAQUS finite element program. Harvard Univ.

Jiang, Z., Guan, Z., Lian, J., 1995. Effects of microstructural variables on the deformation behaviour of dual-phase steel. Materials Science and Engineering: A 190, 55–64. doi:https://doi.org/10.1016/0921-5093(94)09594-M.

Kadkhodapour, J., Butz, A., Rad, S.Z., 2011a. Mechanisms of void formation during tensile testing in a commercial, dual-phase steel. Acta Materialia 59, 2575–2588. doi:https://doi.org/10.1016/j.actamat.2010.12.039.

Kadkhodapour, J., Butz, A., Ziaei-Rad, S., Schmauder, S., 2011b. A micro mechanical study on failure initiation of dual phase steels under tension using single crystal plasticity model. International Journal of Plasticity 27, 1103 – 1125. doi:https://doi.org/10.1016/j.ijplas.2010.12.001.

Lai, Q., Brassart, L., Bouaziz, O., Gouné, M., Verdier, M., Parry, G., Perlade, A., Bréchet, Y., Pardoen, T., 2016. Influence of martensite volume fraction and hardness on the plastic behavior of dual-phase steels: Experiments and micromechanical modeling. International Journal of Plasticity 80, 187–203. doi:https://doi.org/10.1016/j.ijplas.2015.09.006.

Park, K., Nishiyama, M., Nakada, N., Tsuchiyama, T., Takaki, S., 2014. Effect of the martensite distribution on the strain hardening and ductile fracture behaviors in dual-phase steel. Materials Science and Engineering: A 604, 135–141. doi:https://doi.org/10.1016/j.msea.2014.02.058.

Peirce, D., Asaro, R., Needleman, A., 1982. An analysis of nonuniform and localized deformation in ductile single crystals. Acta metallurgica 30, 1087–1119. doi:https://doi.org/10.1016/0001-6160(82)90005-0.

Pierman, A.P., Bouaziz, O., Pardoen, T., Jacques, P., Brassart, L., 2014. The influence of microstructure and composition on the plastic behaviour of dual-phase steels. Acta Materialia 73, 298 – 311. doi:https://doi.org/10.1016/j.actamat.2014.04.015.

Quey, R., Dawson, P., Barbe, F., 2011. Large-scale 3d random polycrystals for the finite element method: Generation, meshing and remeshing. Computer Methods in Applied Mechanics and Engineering 200, 1729–1745. doi:https://doi.org/10.1016/j.cma.2011.01.002.

Shen, H., Lei, T., Liu, J., 1986. Microscopic deformation behaviour of martensitic–ferritic dual-phase steels. Materials science and technology 2, 28–33. doi:https://doi.org/10.1179/mst.1986.2.1.28.

Tasan, C.C., Hoefnagels, J.P., Diehl, M., Yan, D., Roters, F., Raabe, D., 2014. Strain localization and damage in dual phase steels investigated by coupled in-situ deformation experiments and crystal plasticity simulations. International Journal of Plasticity 63, 198–210. doi:https://doi.org/10.1016/j.ijplas.2014.06.004.

Vajragupta, N., Wechsuwanmanee, P., Lian, J., Sharaf, M., Mnstermann, S., Ma, A., Hartmaier, A., Bleck, W., 2014. The modeling scheme to evaluate the influence of microstructure features on microcrack formation of dp-steel: The artificial microstructure model and its application to predict the strain hardening behavior. Computational Materials Science 94, 198 – 213. doi:https://doi.org/10.1016/j.commatsci.2014.04.011. iWCMM23 Special Issue.

Woo, W., Em, V., Kim, E.Y., Han, S., Han, Y., Choi, S.H., 2012. Stress–strain relationship between ferrite and martensite in a dual-phase steel studied by in situ neutron diffraction and crystal plasticity theories. Acta Materialia 60, 6972–6981. doi:https://doi.org/10.1016/j.actamat.2012.08.054.

Yalcinkaya, T., Brekelmans, W., Geers, M., 2008. Bcc single crystal plasticity modeling and its experimental identification. Modelling and Simulation in Materials Science and Engineering 16, 085007. doi:10.1088/0965-0393/16/8/085007.

Yalcinkaya, T., Brekelmans, W.A.M., Geers, M.G.D., 2009. A composite dislocation cell model to describe strain path change effects in BCC metals. Modelling and Simulation in Materials Science and Engineering 17, 064008. doi:10.1088/0965-0393/17/6/064008.

Zecevic, M., Korkolis, Y.P., Kuwabara, T., Knezevic, M., 2016. Dual-phase steel sheets under cyclic tensioncompression to large strains: Experiments and crystal plasticity modeling. Journal of the Mechanics and Physics of Solids 96, 65 – 87. doi:https://doi.org/10.1016/j.jmps.2016.07.003.